2011 American Control Conference
on O'Farrell Street, San Francisco, CA, USA
June 29 - July 01, 2011

Towed-body Trajectory Tracking in Aerial Recovery of Micro Air Vehicle in the presence of Wind

Liang Sun and Randal W. Beard

***Abstract*— This paper presents a method for recovering Micro Air Vehicles (MAVs) in flight using a mothership and towed drogue, in which the mothership executes an orbit that places the drogue in a stable, slower orbit that can be tracked by a MAV. This paper is particularly challenging in the presence of wind. The equations of motion of the cable using an elastic model are presented. Based on the differential flatness of the system with the knowledge of the wind, the desired mothership trajectory can be calculated from the desired drogue orbit. A Lyapunov-based controller derived using backstepping is proposed that enables tracking error of mothership to exponentially converge to an ultimate bound, where the size of the ultimate bound is a function of the unknown portion of the wind. Simulation results verify the feasibility of the approach.**

I. Introduction

In the past decades, Unmanned Aerial Vehicles (UAVs) have been employed for a wide variety of military and civilian applications. The increasingly critical technology and significant information gathered by the UAVs call for protection and retrieval strategies after they complete their missions. Wyllie [1] described a parachute recovery system for fixed wing UAVs. This system has the merits such as mobility, with its ability to land on unprepared ground, but it will be subject to inaccuracies due to wind, and will largely dictate the structural design of the airframe due to the higher landing loads. Kahn [2] developed a vision-based guidance law for small UAV to be recovered by a net on a moving ship. This approach particularly focuses on the landing phase of the UAV within a safe area. To develop a method for a remote instant retrieval in deep enemy territory, Sun et. al. [3] proposed a aerial recovery strategy using a towed-body system. As shown in Figure 1, the basic idea is to maneuver the towplane, or mothership, so that the drogue enters a stable orbit at an airspeed that is slightly below the nominal airspeed of the MAV. The MAV will then be maneuvered to enter the same orbit at its nominal airspeed and will therefore overtake the drogue with a relatively slow closing speed. This paper further extends the aerial recovery approach described in our previous work [3], [4], [5]. The most significant portion to realize a successful recovery using the cable-drogue system is to enable the drogue to enters an easily followed orbit so that the MAV can detect and navigate to the drogue.

Liang Sun, Ph.D student in Department of Electrical and Computer Engineering, Brigham Young University, Provo, UT 84602, USA sun.liang@byu.edu

Randal W. Beard, Professor in Department of Electrical and Computer Engineering, Brigham Young University, Provo, UT 84602, USA beard@byu.edu

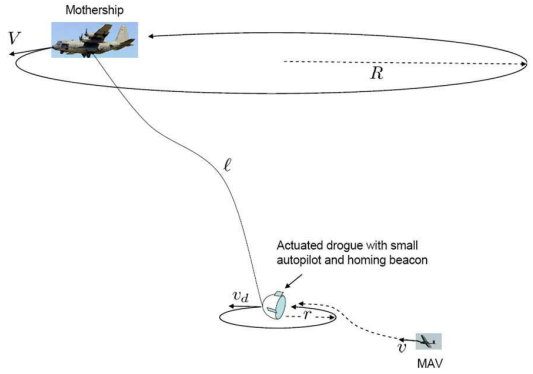

Fig. 1. This figure shows the baseline concept described in the paper. The mothership recovers a MAV by towing a long cable attached to a drogue. The drogue is actuated and can maneuver and communicate with the MAV to facilitate successful capture. The MAV uses missile guidance strategies to intercept the drogue.

The dynamics and stability of circularly towed-cable systems have received attention in the literature. Clifton et. al. [6] explore the steady-state solution of a long wire $(20,000\,ft)$ towed by an aircraft whose airspeed is about $150\,knots$ flying in a circular orbit. It was assumed that the cable is non-elastic, and only small motion around the cable equilibrium position was considered. Bourmistrov et. al. [7] focus on the trajectory tracking control of the towed body while the towing aircraft is assumed to be in straight and level flight with a constant speed and the cable is assumed to be flexible and non-elastic model. A 12-state dynamic equations for the towed body is applied and the nonlinear inversion technique is utilized to develop the control law. Zhu and Rahn [8] derived equations of motion for the perturbed cable-drogue system from steady state. The vibrational equations are linearized and discretized using Galerkin's method and the analysis of the effects of non-dimensional rotation speed, cable fluid drag, cable length, and point mass is presented. More recently, Williams and Trivailo [9] used an object-oriented cable modeling approach to study the relative equilibria of the towed payload system using multiple towplanes.

In this paper, we will continue to explore the trajectory tracking strategy of the drogue in the presence of both known and unknown components of wind. The effect of the wind on the motion of the cable and drogue was first discussed by Murray [10]. Winds cause a steady state offset in the North-East position of the drogue and an oscillation in the altitude direction. Even though the winds are purely in the North

978-1-4577-0079-8/11/$26.00 ©2011 AACC

direction, the drogue is offset in both the North and East direction. This phenomenon was also discussed in [5] based on flight test results. To more precisely match behaviors observed in flight tests, an elastic model of the cable will be developed. Given a desired drogue trajectory, based on the differential flatness of the model with the knowledge of the known component of the wind, we calculate the desired trajectory of the mothership. Figure 2 presents a block diagram of the overall control strategy. Using a mothership dynamic model in the presence of wind, we take a similar approach and develop a Lyapunov-based control law derived using backstepping approach to guarantee the tracking error of the mothership converges exponentially to an ultimate bound where the size of the bound is a function of an upper bound on the unknown component of the wind.

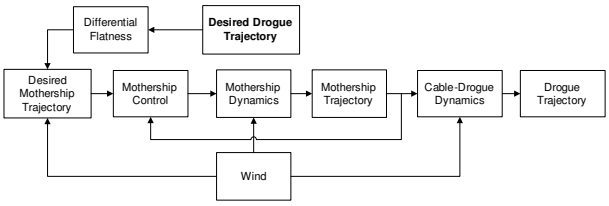

Fig. 2. Strategy diagram for the drogue trajectory tracking in the presence of wind

II. Cable-drogue dynamics

In the literature, the dynamics of towed-body systems are typically modeled by assuming that the cable is flexible and non-elastic [3], [6], [7], [10], [11], [12]. However, in our own flight tests we have observed that the cable stretches considerably [5]. An elastic model for the cable is therefore needed to match simulation results to flight results. Williams and Trivailo [13] developed the equations of the motion of the cable by introducing an elastic model together with two attitude angles at each joint. In this paper, we will develop the cable-drogue dynamics using an elastic model based on Newton's second law. Figure 3 depicts a cable-drogue system

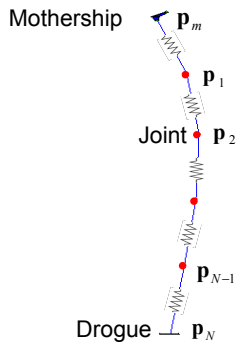

Fig. 3. Cable-drogue systems using spring model

with an $N-$link cable modeled as a finite number point mass nodes connected by springs. The forces acting on each link are lumped together and applied at the joint. The drogue is the last joint of the cable. Let $\mathbf{p}_i \in \mathbb{R}^3$, $i = 1, 2, \cdots, N$, be the location of the ith joint. Based on Newton's second law, the dynamic equations for the drogue are

$$\begin{aligned} m_N \ddot{\mathbf{p}}_N &= \mathbf{T}_N + \Omega_N \\ \Omega_N &= \mathbf{G}_N + \mathbf{D}_N + \mathbf{L}_N, \end{aligned}$$

and the other joints are

$$\begin{aligned} m_{j-1} \ddot{\mathbf{p}}_{j-1} &= \mathbf{T}_{j-1} + \Omega_{j-1} - \mathbf{T}_j \\ \Omega_{j-1} &= \mathbf{G}_{j-1} + \mathbf{D}_{j-1} + \mathbf{L}_{j-1} \\ j &= 2, 3, \cdots, N, \end{aligned}$$

where $m_j, j = 1, 2, \cdots, N$ are the masses of each joint,

$$\begin{aligned} \mathbf{T}_j &= \frac{EA}{\ell_0} \left(\|\mathbf{p}_{j-1} - \mathbf{p}_j\| - \ell_0 \right) \frac{\mathbf{p}_{j-1} - \mathbf{p}_j}{\|\mathbf{p}_{j-1} - \mathbf{p}_j\|}, \\ j &= 1, 2, \cdots, N, \end{aligned}$$

are the elastic tension forces exerted on each joint of the cable, where E is the Young's modulus, A is the cross-sectional area of the cable, $\ell_0 = L_0/N$, where L_0 is the original cable length, $\mathbf{p}_0 = \mathbf{p}_m$, where $\mathbf{p}_m \in \mathbb{R}^3$ is the position of the mothership in the inertial frame, and $\mathbf{G}_j, \mathbf{D}_j, \mathbf{L}_j \in \mathbb{R}^3, j = 1, 2, \cdots, N$ are the gravity, aerodynamic drag and lift forces corresponding to each point mass respectively.

III. Mothership path planning and control in the presence of wind

In [4] we developed a strategy based on differential flatness to regulate the mothership so that the drogue follows a desired trajectory in the absence of wind. In this paper, we will utilize a similar approach but accounting for the presence of wind.

A. Mothership trajectory calculation using differential flatness

Based on the definitions in Section II, suppose that the desired trajectory of the drogue (Nth joint) is C^∞, then the position of the jth mass joint can be calculated as

$$\begin{aligned} \mathbf{p}_{j-1} &= \mathbf{p}_j + \ell \frac{\mathbf{T}_j}{\|\mathbf{T}_j\|}, \\ \mathbf{T}_j &= m_j \ddot{\mathbf{p}}_j - \Omega_j + \mathbf{T}_{j+1}, \\ j &= N, N-1, \cdots, 2, \end{aligned}$$

where $\ell = \ell_0 \left(1 + \frac{\|\mathbf{T}_j\|}{EA}\right)$ and $\mathbf{T}_{N+1} = \mathbf{0}$. At each time step, these equations are applied recursively to each link of the cable until the trajectory of the mothership is calculated. In this paper, we focus on circular trajectories for the drogue.

B. Mothership trajectory tracking in wind

The dynamic equations of the mothership in the presence of wind can be written as

$$\begin{aligned}
\dot{p}_n &= V_a \cos\psi \cos\gamma_a + w_n + N_n && (1)\\
\dot{p}_e &= V_a \sin\psi \cos\gamma_a + w_e + N_e && (2)\\
\dot{p}_d &= -V_a \sin\gamma_a + w_d + N_d && (3)\\
\dot{V}_a &= -g\sin\gamma_a - \frac{D_m}{m_m} + \frac{1}{m_m}u_T + \frac{F_V}{m_m} && (4)\\
\dot{\gamma}_a &= -\frac{g}{V_a}\cos\gamma_a + \frac{g}{V_a}(\cos\phi)u_n + \frac{F_{\gamma_a}}{m_m V_a} && (5)\\
\dot{\psi} &= \frac{L_m}{m_m V_a \cos\gamma_a}\sin\phi + \frac{F_\psi}{m_m V_a \cos\gamma_a} && (6)\\
\dot{\phi} &= u_\phi && (7)
\end{aligned}$$

where $\mathbf{p}_m \triangleq (p_n, p_e, p_d)^T$ is the position of the mothership in the inertial frame, $\mathbf{w}_c \triangleq (w_n, w_e, w_d)^T$ is known component of the wind expressed in the inertial frame, $\mathbf{N}_w \triangleq (N_n, N_e, N_d)^T$ is the unknown component of the wind where we assume that $\|\mathbf{N}_w\| \leq \bar{N}$ where $\bar{N} > 0$, V_a is the magnitude of the airspeed of the mothership,

$$\mathbf{V}_m \triangleq \begin{pmatrix} V_a \cos\psi \cos\gamma_a \\ V_a \sin\psi \cos\gamma_a \\ -V_a \sin\gamma_a \end{pmatrix}$$

is the velocity vector of the airframe relative to the surrounding air, ψ is the heading angle, γ_a is the air mass referenced flight path angle, which is defined as the angle from the inertial North-East plane to the velocity vector of the aircraft relative to the air mass, ϕ is the roll angle, m_m is the mass of the mothership, g is the gravitational constant at Earth sea level, $u_n \triangleq \frac{L_m}{m_m g}$ is the (controlled) load factor, L_m and D_m are the aerodynamic lift and drag forces respectively, u_T is the thrust and $(F_V, F_\psi, F_{\gamma_a})$ are the tension forces in the velocity coordinates. The control inputs are the thrust u_T, the load factor u_n, and the roll angle command u_ϕ. The tension forces in the inertial coordinate system can be expressed in the velocity coordinates via the transformation $(F_V, F_\psi, -F_{\gamma_a})^T = \Gamma \cdot \mathbf{T}_m$, where

$$\Gamma \triangleq \begin{pmatrix} \cos\gamma_a\cos\psi & \cos\gamma_a\sin\psi & -\sin\gamma_a \\ -\sin\psi & \cos\psi & 0 \\ \sin\gamma_a\cos\psi & \sin\gamma_a\sin\psi & \cos\gamma_a \end{pmatrix},$$

and $\mathbf{T}_m$ is defined as the components of tension in the inertial frame for the first cable element connected to the mothership.

Assuming that the desired mothership trajectory $\mathbf{p}_m^c(t) \in \mathbb{R}^3$, which is computed from the desired drogue trajectory using differential flatness, is smooth, and defining the candidate inputs as $\mathbf{u_c} \triangleq (u_T, u_n, \sin\phi)^T$, then rearranging the dynamic equations of the mothership yields

$$\begin{aligned}
\begin{pmatrix} \dot{V}_a \\ \dot{\gamma}_a \\ \dot{\psi} \end{pmatrix} &= \begin{pmatrix} -g\sin\gamma_a - \frac{D_m}{m_m} + \frac{F_v}{m_m} \\ -\frac{g}{V_a}\cos\gamma_a + \frac{F_{\gamma_a}}{m_m V_a} \\ \frac{F_\psi}{m_m V_a \cos\gamma_a} \end{pmatrix} \\
&\quad + \begin{pmatrix} \frac{1}{m_m} & 0 & 0 \\ 0 & \frac{g}{V_a}\cos\phi & 0 \\ 0 & 0 & \frac{L_m}{m_m V_a \cos\gamma_a} \end{pmatrix} \\
&\quad \cdot \begin{pmatrix} u_T \\ u_n \\ \sin\phi \end{pmatrix} \\
&\triangleq \mathbf{F} + \mathbf{G}\mathbf{u}_c.
\end{aligned}$$

Theorem 3.1 *Consider the system with the dynamic equations (1) - (7) under the stated definitions and assumptions, let*

$$\xi \triangleq -(\mathbf{MG})^{-1}\left(\mathbf{e}_m + \mathbf{MF} - \ddot{\mathbf{p}}_m^c + k_1\dot{\mathbf{e}}_m - k_2\mathbf{z}_m^{\mathbf{e}}\right) \quad (8)$$

where

$$\mathbf{e}_m \triangleq \mathbf{p}_m - \mathbf{p}_m^c, \quad (9)$$

$$\mathbf{M} \triangleq \begin{pmatrix} \cos\gamma_a\cos\psi & -V_a\sin\gamma_a\cos\psi \\ \cos\gamma_a\sin\psi & -V_a\sin\gamma_a\sin\psi \\ -\sin\gamma_a & -V_a\cos\gamma_a \\ -V_a\cos\gamma_a\sin\psi & \\ -V_a\cos\gamma_a\cos\psi & \\ 0 & \end{pmatrix}$$

$$\mathbf{z}_m^{\mathbf{e}} \triangleq -\mathbf{V}_m - \mathbf{w}_c + \dot{\mathbf{p}}_m^c - k_1\mathbf{e}_m, \quad (10)$$

and select the control inputs as

$$\begin{pmatrix} u_T \\ u_n \end{pmatrix} = \begin{pmatrix} 1 & 0 & 0 \\ 0 & 1 & 0 \end{pmatrix}\xi \quad (11)$$

$$u_\phi = \frac{1}{\cos\phi}\left(\begin{pmatrix} 0 & 0 & 1 \end{pmatrix}\dot{\xi} + (\mathbf{z}_m^{\mathbf{e}})^T\mathbf{MG}\begin{pmatrix} 0 \\ 0 \\ 1 \end{pmatrix} - k_3 z_m^\phi\right) \quad (12)$$

where

$$z_m^\phi \triangleq \sin\phi - \begin{pmatrix} 0 & 0 & 1 \end{pmatrix}\xi.$$

Suppose that $\mathbf{p}_m^c(t) = (p_n, p_e, p_d)^T$ *is a sufficiently smooth time-varying trajectory with bounded derivatives. Then, if the constants* k_1, k_2 *and* k_3 *are positive, then the tracking error* $\mathbf{e}_m$ *has a uniform ultimated bound* $\bar{N}/\sqrt{\lambda\sigma}$, *where*

$$\sigma = \min\left\{2k_1,\ (\min\{k_1,\ k_2,\ k_3\})^2\right\} \quad (13)$$

$$\lambda = \min\left\{1,\ 2\cdot\min\left\{\left(k_1 - \frac{\sigma}{2}\right),\ k_2,\ k_3\right\}\right\}. \quad (14)$$

Proof:

Step 1. Error dynamics: The dynamic equation for the inertial tracking error from Equation (9) is given by

$$\dot{\mathbf{e}}_m = \dot{\mathbf{p}}_m - \dot{\mathbf{p}}_m^c = \mathbf{V}_m + \mathbf{w}_c + \mathbf{N}_w - \dot{\mathbf{p}}_m^c.$$

Step 2. Error convergence: Define the Lyapunov function candidate $V_1 \triangleq \frac{1}{2}\mathbf{e}_m^T\mathbf{e}_m$, which has time derivative

$$\dot{V}_1 = \mathbf{e}_m^T\left(\mathbf{V}_m + \mathbf{w}_c + \mathbf{N}_w - \dot{\mathbf{p}}_m^c\right).$$

Introducing the error variable (10), we have

$$\dot{V}_1 = -k_1\mathbf{e}_m^T\mathbf{e}_m - \mathbf{e}_m^T\left(\mathbf{z}_m^{\mathbf{e}}\right) + \mathbf{e}_m^T\mathbf{N}_w.$$

Step 3. Backstepping for $\mathbf{z}_m^{\mathbf{e}}$: Consider the augmented Lyapunov function candidate

$$V_2 \triangleq V_1 + \frac{1}{2}\left(\mathbf{z}_m^{\mathbf{e}}\right)^T\left(\mathbf{z}_m^{\mathbf{e}}\right),$$

with time derivative

$$\begin{aligned}\dot{V}_2 &= -k_1\mathbf{e}_m^T\mathbf{e}_m + \left(\mathbf{z}_m^{\mathbf{e}}\right)^T\left(-\mathbf{e}_m - \dot{\mathbf{V}}_m + \ddot{\mathbf{p}}_m^c\right.\\ &\quad \left.-k_1\dot{\mathbf{e}}_m\right) + \mathbf{e}_m^T\mathbf{N}_w.\end{aligned}$$

From the mothership dynamic equations we have $\dot{\mathbf{V}}_m = \mathbf{M}\left(\mathbf{F} + \mathbf{G}\mathbf{u}_c\right)$. Therefore

$$\begin{aligned}\dot{V}_2 &= -k_1\mathbf{e}_m^T\mathbf{e}_m + \left(\mathbf{z}_m^{\mathbf{e}}\right)^T\left(-\mathbf{e}_m - \mathbf{M}\mathbf{F} - \mathbf{M}\mathbf{G}\mathbf{u}_c\right.\\ &\quad \left.+\ddot{\mathbf{p}}_m^c - k_1\dot{\mathbf{e}}_m\right) + \mathbf{e}_m^T\mathbf{N}_w.\end{aligned}$$

It can be seen that $\mathbf{MG}$ is invertible[1], therefore using (8) and defining $\eta \triangleq \sin\phi$ and supposing that u_T and u_n are selected as in (11), then the time derivative of the z_m^{ϕ} is $\dot{z}_m^{\phi} = u_\phi\cos\phi - \begin{pmatrix}0 & 0 & 1\end{pmatrix}\dot{\xi}$, and

$$\mathbf{u}_c = \begin{pmatrix} u_T \\ u_n \\ \eta \end{pmatrix} = \xi + z_m^{\phi}\begin{pmatrix} 0 \\ 0 \\ 1 \end{pmatrix}.$$

Thus

$$\begin{aligned}\dot{V}_2 &= -k_1\mathbf{e}_m^T\mathbf{e}_m - k_2\left(\mathbf{z}_m^{\mathbf{e}}\right)^T\left(\mathbf{z}_m^{\mathbf{e}}\right)\\ &\quad + \left(\mathbf{z}_m^{\mathbf{e}}\right)^T\left(-\mathbf{M}\mathbf{G}\begin{pmatrix}0\\0\\1\end{pmatrix}z_m^{\phi}\right) + \mathbf{e}^T\mathbf{N}_w.\end{aligned}$$

Step 4. Backstepping for z_m^{ϕ}: Consider the augmented Lyapunov function candidate

$$V_3 \triangleq V_2 + \frac{1}{2}\left(z_m^{\phi}\right)^2 = \frac{1}{2}\left\|\mathbf{e}_m\right\|^2 + \frac{1}{2}\left\|\mathbf{z}_m^{\mathbf{e}}\right\|^2 + \frac{1}{2}\left(z_m^{\phi}\right)^2 \quad (15)$$

with time derivative

$$\begin{aligned}\dot{V}_3 &= -k_1\mathbf{e}_m^T\mathbf{e}_m - k_2\left(\mathbf{z}_m^{\mathbf{e}}\right)^T\left(\mathbf{z}_m^{\mathbf{e}}\right)\\ &\quad + z_m^{\phi}\left(u_\phi\cos\phi - \begin{pmatrix}0 & 0 & 1\end{pmatrix}\dot{\xi}\right.\\ &\quad \left. - \left(\mathbf{z}_m^{\mathbf{e}}\right)^T\mathbf{M}\mathbf{G}\begin{pmatrix}0\\0\\1\end{pmatrix}\right) + \mathbf{e}^T\mathbf{N}_w.\end{aligned}$$

If u_ϕ is given by (12), then the time derivative of V_3 becomes

$$\dot{V}_3 = -k_1\mathbf{e}_m^T\mathbf{e}_m - k_2\left(\mathbf{z}_m^{\mathbf{e}}\right)^T\left(\mathbf{z}_m^{\mathbf{e}}\right) - k_3(z_m^{\phi})^2 + \mathbf{e}^T\mathbf{N}_w. \quad (16)$$

Step 5. Ultimate bound: From Equation (16), we obtain

$$\dot{V}_3 \le -k_1\left\|\mathbf{e}_m\right\|^2 - k_2\left\|\mathbf{z}_m^{\mathbf{e}}\right\|^2 - k_3\left(z_m^{\phi}\right)^2 + \left\|\mathbf{e}_m\right\|\left\|\mathbf{N}_w\right\|.$$

Defining the vector $\mathbf{Y} \triangleq \left(\left(\mathbf{e}_m\right)^T, \left(\mathbf{z}_m^{\mathbf{e}}\right)^T, z_m^{\phi}\right)^T$, and letting $0 < \mu \le \min\{k_1,\, k_2,\, k_3\}$, we have $\dot{V}_3 \le -\mu\left\|\mathbf{Y}\right\|^2 + \left\|\mathbf{Y}\right\|\left\|\mathbf{N}_w\right\|$. To use the term $\mu\left\|\mathbf{Y}\right\|^2$ to dominate $\left\|\mathbf{Y}\right\|\left\|\mathbf{N}_{\mathbf{w}}\right\|$, we rewrite the foregoing inequality as

$$\dot{V}_3 \le -\mu\left(1-\theta\right)\left\|\mathbf{Y}\right\|^2 - \mu\theta\left\|\mathbf{Y}\right\|^2 + \left\|\mathbf{Y}\right\|\left\|\mathbf{N}_w\right\|,$$

where $0 < \theta < 1$. The term $-\mu\theta\left\|\mathbf{Y}\right\|^2 + \left\|\mathbf{Y}\right\|\left\|\mathbf{N}_w\right\|$ will be less than zero if $\left\|\mathbf{Y}\right\| \ge \frac{\left\|\mathbf{N}_w\right\|}{\mu\theta}$. From the input-to-state stability theorem [14], it can be concluded that

$$\left\|\mathbf{Y}\right\| \le \beta\left(\left\|\mathbf{Y}\left(t_0\right)\right\|, t - t_0\right) + \gamma\left(\sup_{t_0\le\tau\le t}\mathbf{N}_w\left(\tau\right)\right),$$

where β is a class $\mathcal{KL}$ function and γ is a class $\mathcal{K}$ function defined as $\gamma\left(r\right) \triangleq \frac{r}{\mu\theta}$. Therefore, according to the Lyapunov stability theorem [14], $\left\|\mathbf{Y}\right\|$ is uniformly ultimately bounded, and since $\left\|\mathbf{e}_m\right\| \le \left\|\mathbf{Y}\right\|$, $\left\|\mathbf{e}_m\right\|$ is also uniformly ultimately bounded within a ball of radius $\bar{N}/\mu\theta$.

Step 6. Exponential convergence: By using the Young's inequality[2], it can be concluded that for any $\sigma > 0$

$$\begin{aligned}\dot{V}_3 &\le -\left(k_1 - \frac{\sigma}{2}\right)\left\|\mathbf{e}_m\right\|^2 - k_2\left\|\mathbf{z}_m^{\mathbf{e}}\right\|^2\\ &\quad -k_3\left(z_m^{\phi}\right)^2 + \frac{1}{2\sigma}\left\|\mathbf{N}_w\right\|^2.\end{aligned}$$

Suppose we choose $0 < \sigma < 2k_1$ so that the term $k_1 - \frac{\sigma}{2}$ is positive. Then we can conclude that there is a sufficiently small positive constant λ satisfying

$$0 < \frac{\lambda}{2} \le \min\left\{\left(k_1 - \frac{\sigma}{2}\right),\, k_2,\, k_3\right\}$$

such that

$$\dot{V}_3 \le -\lambda V_3 + \frac{1}{2\sigma}\bar{N}^2,$$

therefore, it can be concluded from the Comparison Lemma [14] that

$$V_3\left(t\right) \le e^{-\lambda t}V_3\left(0\right) + \frac{1}{2\lambda\sigma}\bar{N}^2,\ t \ge 0.$$

Then all signals remain bounded and therefore the solution exists globally. Moreover, V_3 converges to a ball of radius $\bar{N}^2/\left(2\lambda\sigma\right)$ and $\mathbf{e}_m$ converges exponentially to a ball of radius $\bar{N}/\sqrt{\lambda\sigma}$ because of (15).

Selecting σ and λ using (13) and (14), we pick $\theta = \sqrt{\lambda}$ and $\mu = \sqrt{\sigma}$ to guarantee that the ultimate bound is $\bar{N}/\sqrt{\lambda\sigma}$. □

IV. Simulation results

Consistent with the configuration of the preliminary flight test [5], the following parameters and operational boundaries are used in the simulation: (1) mothership (a twin prop, 55-inch wingspan, battery-powered, autonomous aircraft with Kestrel autopilot): $m_m = 1.76\,kg$, $12\,m/s \le V_a \le 20\,m/s$, $-35 \le \phi \le 35°$, $-15° \le \gamma_a \le 35°$, lift coefficient $C_{L_m} = 0.28$, drag coefficient $C_{D_m} = 0.06$, wing area $S_m = 0.307\,m^2$; (2) drogue (hemisphere with Kestrel autopilot): mass $m_{dr} = 0.11\,kg$, lift coefficient $C_{L_{dr}} = 0.02$, drag

[1] By constraining V, γ, and χ to reasonable values, the matrices $\mathbf{M}$ and $\mathbf{G}$ will be full rank. The product of two full-rank matrices is also full rank.

[2] A special case of the Young's inequality is $ab \le (\gamma/2)\,a^2 + (1/2\gamma)\,b^2$, where $a,\ b \ge 0$, and γ is any positive constant.

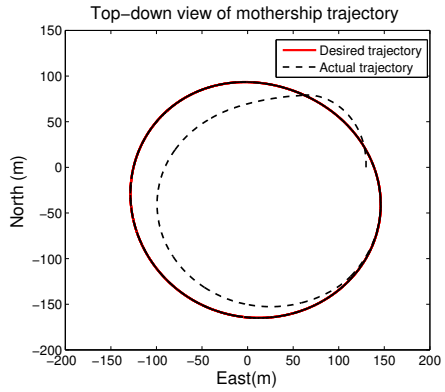

Fig. 4. Top-down view of mothership trajectory in the presence of wind.

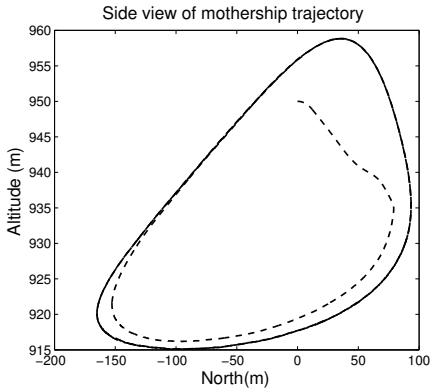

Fig. 5. North-altitude view of mothership trajectory in the presence of wind.

coefficient $C_{D_{dr}} = 0.2$, wing area $S_{dr} = 0.1\,m^2$; (3) cable (fishing line): mass $m_c = 0.01\,kg$, $L_0 = 110\,m$, links $N = 5$, diameter $d = 0.00041\,m$, Young's modulus $E = 1.904 \times 10^9\,N/m^2$.

Given a desired drogue trajectory, the desired mothership trajectory can be calculated using the approach in III-A. Savitzky-Golay filter [15] was applied to locally smooth the velocity and acceleration computations in which the process is to compute the entire trajectory history of a given link and then smooth the trajectory to remove high frequency numerical noise before computing the trajectory of the next link [10].

A desired circular trajectory of the drogue can be written in parametric form as $p_n^{dr}(t) = R^{dr}\sin\left(\frac{V^{dr}}{R^{dr}}t\right)$, $p_e^{dr}(t) = R^{dr}\cos\left(\frac{V^{dr}}{R^{dr}}t\right)$, $p_d^{dr}(t) = -900\,\text{m}$, $t \in [0, +\infty)$, where $(p_n^{dr}, p_e^{dr}, p_d^{dr})^T$ are the coordinates of the drogue in North-East-Down (NED) coordinates, R^{dr} and V^{dr} are the desired orbit radius and ground speed of the drogue respectively. Due to the operational boundaries of the mothership, given a constant wind component, we have to tune R^{dr} and V^{dr} to derive a feasible trajectory for the mothership to track. For a constant wind speed vector $\mathbf{w}_c = (5, 0, 0)^T\,m/s$, R^{dr} and V^{dr} can be selected as $110\,m$ and $13\,m/s$. The control gains are selected as $k_1 = 0.3$, $k_2 = 4$, $k_3 = 20$. The bound on the wind gusts can be given by $\bar{N} = 0.5\,m/s$, therefore the ultimate bound can be calculated as $2.33\,m$. The initial positions of the mothership and drogue are $(0, 130, -950)^T\ m$ and $(0, 130, -840)^T\ m$ respectively in NED coordinates.

Figure 4 shows the North-East view of the mothership trajectory, in which it can be seen that the mothership follows the desired trajectory precisely after one circle of the orbit. Figure 5 shows the North-altitude view of the mothership trajectory, in which we can see the large inclined orbit of the mothership. As mentioned in [10], even though the mothership flies a flat orbit the presence of wind causes the orbit of the drogue to be inclined. Therefore, to compensate for the oscillation of the drogue altitude, the mothership must incline its orbit. Figure 6 shows the error of the mothership. Although the mothership has an original offset from desired

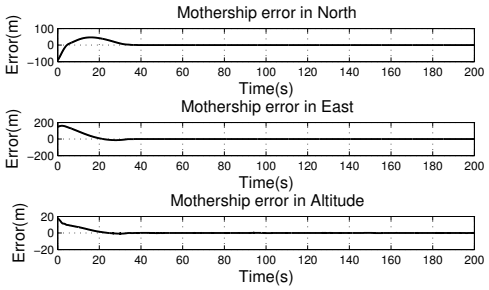

Fig. 6. Mothership trajectory error in the presence of wind.

position, after 30 seconds, all the tracking errors converges to a neighborhood of the origin. Figure 7 shows the top-down view of the drogue trajectory. It can be seen that it takes longer for the drogue to converge to desired orbit than the mothership. This is because of the flexible connection between the mothership and the drogue, which delays the response of the drogue.

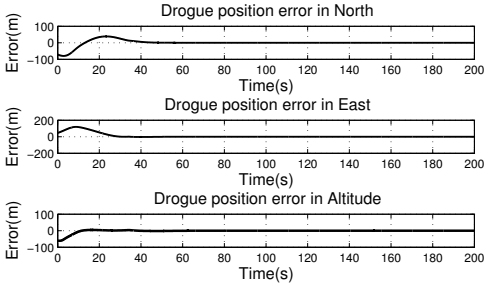

Fig. 8. Drogue trajectory error in the presence of known wind.

Figure 8 gives the tracking errors of the drogue. It can be seen that after the mothership tracking errors converge to a neighborhood of the origin ($t > 30\,s$), the drogue tracking errors also enter a neighborhood of the origin ($t > 40\,s$). The delayed responding time (about $10\,s$ in the current simulation) of the drogue will vary with the different initial positions of the mothership. Figure 9 shows the evolution of the roll angle ϕ, the path angle γ_a, the thrust T and the

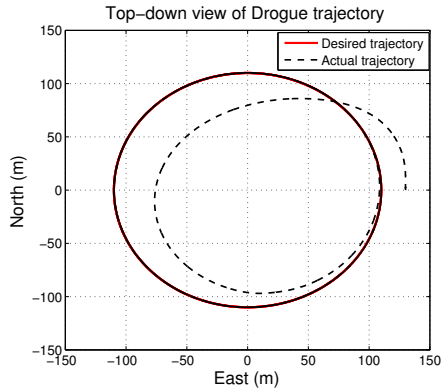

Fig. 7. Top-down view of drogue trajectory in the presence of wind.

load factor n of the mothership during flight. Because of the inclined orbit of the mothership, it has to fly up and down explaining the oscillation of path angle and the load factor. Since the constant wind dominates the noise, to keep a constant ground speed, the mothership regulates its airspeed to mitigate the effect of wind during flight explaining the oscillation of the mothership thrust. Figure 10 shows the magnitude of the mothership tracking error converges within its ultimate bound after 40 seconds.

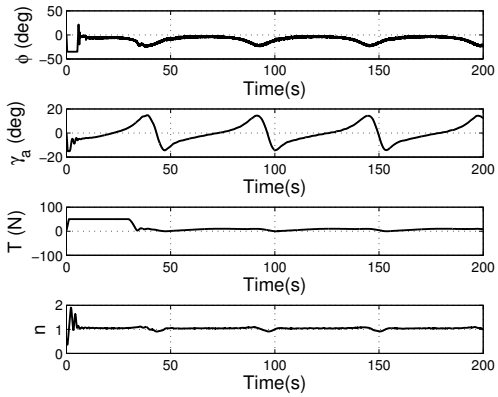

Fig. 9. Time evolution of the roll angle ϕ, path angle γ_a, thrust T and the load factor n of the mothership in the presence of wind.

V. Conclusion

In this paper we developed the equations of motion for a cable-drogue system directly accounting for the elasticity of the cable. An inverse dynamics method based on the differential flatness of the system was used to calculate the required mothership orbit to achieve a desired drogue orbit. Using a Lyapunov-based backstepping approach, the control law was designed to enable the tracking error of the mothership to converge exponentially to an ultimate bound where the size of the bound is proportional to the strength of the unknown wind. Simulation results showed the feasibility of the strategy.

VI. Acknowledgment

This research was supported by the Air Force Office of Scientific Research under STTR contract No. FA 9550-09-C-0102 to Procerus Technologies and Brigham Young University.

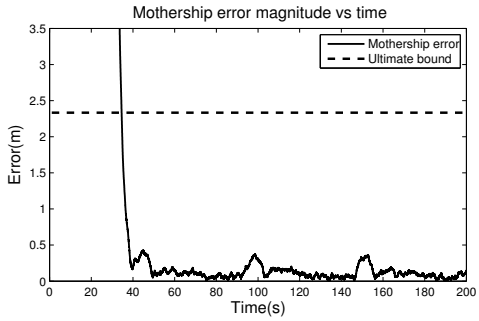

Fig. 10. Time evolution of the magnitude of the tracking error of the mothership in the presence of wind.

References

[1] T. Wyllie, "Parachute recovery for uav systems," *Aircraft Engineering and Aerospace Technology*, vol. 73, no. 6, pp. 542–551, 2001.

[2] A. D. Kahn, "Vision-based recovery and guidance for small unmanned air vehicles." Toronto, Ontario Canada: AIAA Guidance, Navigation, and Control Conference, August 2010.

[3] L. Sun, R. W. Beard, M. B. Colton, and T. W. McLain., "Dynamics and control of cable-drogue system in aerial recovery of micro air vehicles based on gauss's principle." St. Louis, MO, USA: 2009 American Control Conference, June 2009, pp. 4729–4734.

[4] L. Sun, R. W. Beard, and M. B. Colton, "Motion planning and control for mothership-cable-drogue systems in aerial recovery of micro air vehicles." Baltimore, MD, USA: American Control Conference (ACC), 2010, pp. 2101 – 2106.

[5] L. Sun and R. W. Beard, "Towed body altitude stabilization and states estimation in aerial recovery of micro air vehicles." Toronto, Ontario Canada: AIAA, Guidance, Navigation and Control Conference, August 2010.

[6] J. M. Clifton, L. V. Schmidt, and T. D. Stuart, "Dynamic modeling of a trailing wire towed by an orbiting aircraft," *Journal of Guidance, Control and Dynamics*, vol. 18, no. 4, pp. 875–881, 1995.

[7] A. S. Bourmistrov, R. D. Hill, and P. Riseborough, "Nonlinear control law for aerial towed target," *Journal of Guidance Control and Dynamics*, vol. 18, no. 6, pp. 1232–1238, 1995.

[8] F. Zhu and C. D. Rahn, "Stability analysis of a circularly towed cable-body system," *Journal of Sound and Vibration*, vol. 217, no. 3, pp. 435–452, May 1998.

[9] P. Williams and W. Ockels, "Dynamics of towed payload system using multiple fixed-wing aircraft," *Journal of guidance, control, and dynamics*, vol. 32, no. 6, pp. 1766–1780, November-Decemeber 2009.

[10] R. Murray, "Trajectory generation for a towed cable system using differential flatness," *13th Triennial World Congress of the International Federation of Automatic Control*, pp. 395–400, 1996.

[11] J. Cochran, M. Innocenti, T. No, and A. Thukral, "Dynamics and control of maneuverable towed flight vehicles," *JGCD*, vol. 15, no. 5, pp. 1245–1252, 1992.

[12] J. E. Quisenberry and A. S. Arena, "Dynamic simulation of low altitude aerial tow systems," in *AIAA Atmospheric Flight Mechanics Conference and Exhibit*, vol. 1, Providence, Rhode Island, August 2004, pp. 243–252.

[13] P. Williams and P. Trivailo, "Dynamics of circularly towed cable systems, part 1: Optimal configurations and their stability," *AIAA Journal of Guidance Control and Dynamics*, vol. 30, no. 3, pp. 753–765, May-June 2007.

[14] H. K. Khalil, *Nonlinear Systems*, 3rd ed. Upper Saddle River, NJ: Prentice Hall, 2002.

[15] S. Orfanidis, *Introduction to Signal Processing*. Prentice-Hall, 1996.